Check for updates

ASCE

Hybrid Simulation of Structure-Pipe-Structure Interaction within a Gas Processing Plant

Ziliang Zhang[1]; Jamin Park, Ph.D.[2]; Oh-Sung Kwon, Ph.D., P.Eng., M.ASCE[3]; Anastasios Sextos, Ph.D., M.ASCE[4]; Elias Strepelias, Ph.D.[5]; Nikolaos Stathas, Ph.D.[6]; and Stathis Bousias, Ph.D.[7]

Abstract: Though often overlooked, the impact of seismic transient ground deformation on natural gas (NG) pipes can be highly adverse. Particularly, pipe elbows may undergo excessive in-plane bending demand and buckling. In this paper, a critical scenario of a pipe coupling two industrial structures typically found in an NG processing plant is studied. High strain and cross-sectional ovalization on the elbows are probable during an earthquake due to the out-of-phase oscillation of the two structures imposing asynchronous displacement demands at the two pipe ends. A parametric study was first performed to investigate various structure-pipe-structure configurations that increase seismic demands to pipe elbows. Simultaneous mobilization of divergent oscillation between two supporting structures at the low-frequency range, a lower pipe-structure stiffness ratio, a shorter length of straight pipe segments in the linking pipe element, and a higher pipe internal pressure have led to the onset of critical strain demands in pipe elbows. To validate this observation, an experimental campaign was developed in which a full-scale linking pipe element was physically tested by means of hybrid simulation (HS). The study shows that the seismic interaction of the structures coupled with the pipe is nonnegligible and can even be critical for the integrity of the coupling pipe. The finding depends on the structural system's dynamic and geometrical properties as well the frequency content of the earthquake excitation. **DOI: 10.1061/(ASCE)PS.1949-1204.0000526.** *© 2020 American Society of Civil Engineers.*

Introduction

Natural gas (NG) constitutes a significant percentage of current global energy consumption. Its demand has increased over the last decade and is expected to proliferate into the future with increased global interest in clean energy (DOE 2017; Sextos et al. 2018). Among many factors, transport and supply play an essential role in the NG industry, which includes transmission, storage, gas liquefaction, and regasification (GIE 2015). Since NG reserves are commonly distant from consumer markets, the need for delivering NG to end-users has led to the world's mass construction of complex lifeline systems with numerous integrated components and processes. In 2019, the annual regasification capacity of large-scale liquefied natural gas (LNG) terminals in Europe came to 241 billion $\mathrm{m}^3(\mathrm{N})/\mathrm{year}$ and capacity expansion of another 140 billion $\mathrm{m}^3(\mathrm{N})/\mathrm{year}$ was planned (GIE 2019). Along with their clear economic and strategic importance, NG facilities are often associated with high natural and man-made risks. As a result, gas infrastructure security and safety has always been the core value of NG transmission facilities such as LNG terminals, compression stations, peak sheaving stations, pressure let-down stations, and blending stations, which are vulnerable to natural hazards such as earthquakes. In the last decade, natural hazard triggering technological accidents (Na-Tech), and more specifically seismic Na-Tech, has been slowly accepted as a fundamental contribution to the overall risk assessment figures calculated by considering solely industrial accidents (Lanzano et al. 2015). Past Na-Tech disasters have displayed such devastating consequences in causing substantial social, economic, and environmental loss that the future prevention of loss of containment events in critical infrastructures is clearly an issue of major importance (Nakashima et al. 2014).

Pipe elbows are critical components to the safety of pipe within NG processing plants. Compared to straight pipe segments with the identical cross section specification and material properties, the elbows are more flexible and associated with significantly higher stresses, strains, and cross-sectional ovalization (Karamanos 2016). To date, code prescriptions of seismic design for pipelines are generally scarce. In European Committee for Standardization (CEN) *Eurocode 8*, for example, principal guidelines were provided for above-ground pipeline in accordance with generic seismic design approaches (CEN 2006). In terms of research, much effort has been devoted on dynamic analysis of above-ground pipe elbows, mostly in the form of cyclic bending analysis of individual elbow members in which their failure mode under extreme loading conditions were heavily investigated both numerically and experimentally. The most reported elbow damage pattern was the axial development

[1]Ph.D. Candidate, Dept. of Civil Engineering, Univ. of Bristol, Queen's Bldg., University Walk, Bristol BS8 1TR, UK. Email: zz17635@bristol.ac.uk

[2]Postdoctoral Research Fellow, Dept. of Civil and Mineral Engineering, Univ. of Toronto, Toronto, ON, Canada M5S 1A4. Email: jamin.park@utoronto.ca

[3]Professor, Dept. of Civil and Mineral Engineering, Univ. of Toronto, Toronto, ON, Canada M5S 1A4. ORCID: https://orcid.org/0000-0002-3292-9194. Email: os.kwon@utoronto.ca

[4]Professor, Dept. of Civil Engineering, Univ. of Bristol, Queen's Bldg., University Walk, Bristol BS8 1TR, UK (corresponding author). ORCID: https://orcid.org/0000-0002-2616-9395. Email: a.sextos@bristol.ac.uk

[5]Postdoctoral Research Fellow, Structures Laboratory, Dept. of Civil Engineering, Univ. of Patras, Patras 26504, Greece. Email: ilstrepelias@upatras.gr

[6]Postdoctoral Research Fellow, Structures Laboratory, Dept. of Civil Engineering, Univ. of Patras, Patras 26504, Greece. ORCID: https://orcid.org/0000-0002-5694-8779. Email: stathas@upatras.gr

[7]Professor, Director of Structures Laboratory, Dept. of Civil Engineering, Univ. of Patras, Patras 26504, Greece. Email: sbousias@upatras.gr

Note. This manuscript was submitted on May 17, 2020; approved on September 8, 2020; published online on December 24, 2020. Discussion period open until May 24, 2021; separate discussions must be submitted for individual papers. This paper is part of the ***Journal of Pipeline Systems Engineering and Practice***, © ASCE, ISSN 1949-1190.

of through-wall cracks near elbow flanks due to low cycle fatigue accompanied by ratcheting effect (Hasegawa et al. 2008; Hassan et al. 2015; Jeon et al. 2017; Karvelas et al. 2019; Nakamura and Kasahara 2016, 2017; Varelis et al. 2012; Watakabe et al. 2017), while evidence of local buckling followed by crack development has also been mentioned (Hasegawa et al. 2008).

Investigations also went into complex pipe systems coupled within industrial structures and plants. Reza et al. (2013) investigated, by means of hybrid simulation (HS), the seismic performance of a full-scale pipe system coupled within a single industrial building. The pipe system is located on the top level of a 3-story steel structure and is connected to a number of storage tanks and devices inside the structure. Test results showed that even with the maximum earthquake input under their investigation, the pipeline system remained below the yield limit at all locations. The authors of this paper believed that excessive strain development on pipe was inhibited because all supporting points of the pipe was contained on the same floor of the same structure, which is likely to respond synchronously during the earthquake. We stress that this would not necessarily be the case if different support points of the pipe (in a single structure, between multiple structures, or between a structure and the free field) vibrated out-of-phase.

For above-ground pipes, Sakai et al. (2013) evaluated the safety of a piping system using HS, in which a 90° elbow was physically tested and the remainder of the pipeline system was simulated in a coupled numerical model. Permitting the assumption that one end of the elbow specimen was fully fixed onto the laboratory floor, and therefore had zero motion, the test concluded that the 8-in. diameter uniform wall-thinning elbow can fail in the form of low cyclic fatigue under certain conditions. Vathi et al. (2017) simulated the seismic performance of a pipe system and its associated pipe rack and liquid storage tank within an industrial plant. After undergoing seismic excitation, it was found that the critical component of the pipe system was the upper elbow located at the top of a pipe rack, where local strain value exceeded the limit of severe plastification. The differential motion between the ground surface and the structural response on top of the pipe rack where the pipe was elevated made possible the asynchronous displacements at two ends of the elbow, hence the conspicuous elbow in-plane bending. Sextos et al. (2017) examined numerically the seismic performance of mechanical subsystems within a nuclear power plant containment structure using refined finite-element models. It was found that under certain circumstances, elbows were susceptible to significantly increased seismic demand if geometrical nonlinearities introduced by the effects of structure rocking and sliding with uplift are considered. Wenzel et al. (2018) analyzed the nonlinear behavior of a coupled foundation tank–pipeline system using HS, in which a liquid storage tank and its base-isolated foundation were simulated numerically and a small portion of pipe connected directly to the tank was tested physically. Under the assumption that the far end of the physical pipe specimen was fully fixed to the laboratory floor, a significant displacement time history was exerted onto the physical pipe specimen during the HS. The result showed that the critical component was one of the elbows located near heavy auxiliary masses on pipe. Bursi et al. (2018) numerically evaluated the nonlinear response of a whole LNG plant under moderate seismic loading. The study found elbows on top of the tall LNG storage tank were the critical components in the loop and can exhibit a high degree of vulnerability during transient ground motions. This was because of the high differential displacement between the pipe rack and the pump columns located over the dome of the storage tank.

Similarly, for buried NG pipelines, the impact of out-of-phase oscillation induced by differential earthquake inputs has been highlighted previously. Psyrras et al. (2019, 2020) numerically and experimentally investigated the seismic risk of buried NG pipelines when subjected to spatially varying transient ground deformations. Results showed that even for straight buried pipelines, the seismic vibrations at the vicinity of laterally inhomogeneous sites can produce differential movements on different locations of a long pipeline due to kinematic soil-pipe interaction. As a result, appreciable axial stress concentration can be observed in the critically affected pipeline segment near the soil material discontinuity, high enough to trigger coupled buckling modes into the plastic range.

Notwithstanding the aforementioned advancements, there are still several clear limitations in the existing literature. While many studies investigate the seismic demand of pipe coupled to its surroundings, rarely had a set of realistic boundary conditions been successfully adopted to a realistic seismic scenario in which differential displacement between the two pipe ends of an above-ground pipe was significant. It was not uncommon in previous studies that researchers employed overbold assumptions regarding boundary conditions of the pipe supports, such as full constraint (zero motion) at one end of the investigated pipe, whereas in reality any pipe support connected to another entity should have the corresponding motion at the boundary. For example, the base of a pipe support anchored onto the ground surface would be subjected to the same excitation as the foundation input motion exerted to nearby structures. This level of boundary condition accuracy is the (bare) minimum that should be adopted in any modeling practices of above-ground pipes, regardless of considering or neglecting any potential coupling effect. Further more, the importance of structure coupling in industrial NG plants due to the existence of pipes extending between them has not yet been addressed. It is unclear that to what extent the negligence of structural coupling introduced by bridging NG pipes can affect their design prospect. Should the interaction leads to detrimental effects, whether buckling failure or other forms of damage can occur on the pipes or the coupled structures during transient ground motion, awaits investigation. Finally, how the coupling effect is influenced by the various properties of the pipe and those of the supporting industrial structures, as well as the characteristic of the input earthquake excitation remains in doubt.

Along these lines, the objectives of this paper are:

- To identify key parameters of the coupling problem within the proposed structure-pipe-structure configuration, and illustrate the sensitivity of both the global structural response and the induced local elbow demand to these parameters and their most critical combination, by means of finite-element analysis (FEA); and
- To experimentally examine the damage potential of pipe when it is subjected to the differential displacement between two pipe ends by means of HS, given that the difficulties associated with numerically modeling geometrical nonlinearities of pressurized pipe with buckling potential, the effect of nonnegligible structure-pipe-structure interaction, and the scale of the industrial structures involved in the proposed scenario.

Problem Studied

The scenario examined herein consists of two realistic industrial building configurations: supporting Structure A is a three-story NG compressor house, and supporting Structure B is an exposed platform topped with two tall and heavy reliquefication condensers on its deck [Fig. 1(a)]. Both structures are steel moment-resisting frames with reinforced concrete slabs and are assumed to behave elastically. They have first-mode natural frequencies of $f_A = 3.3$ Hz and $f_B = 2.3$ Hz, respectively; hence, a structural frequency ratio is $f_B/f_A = 0.7$. There is an NG pipe behaving as

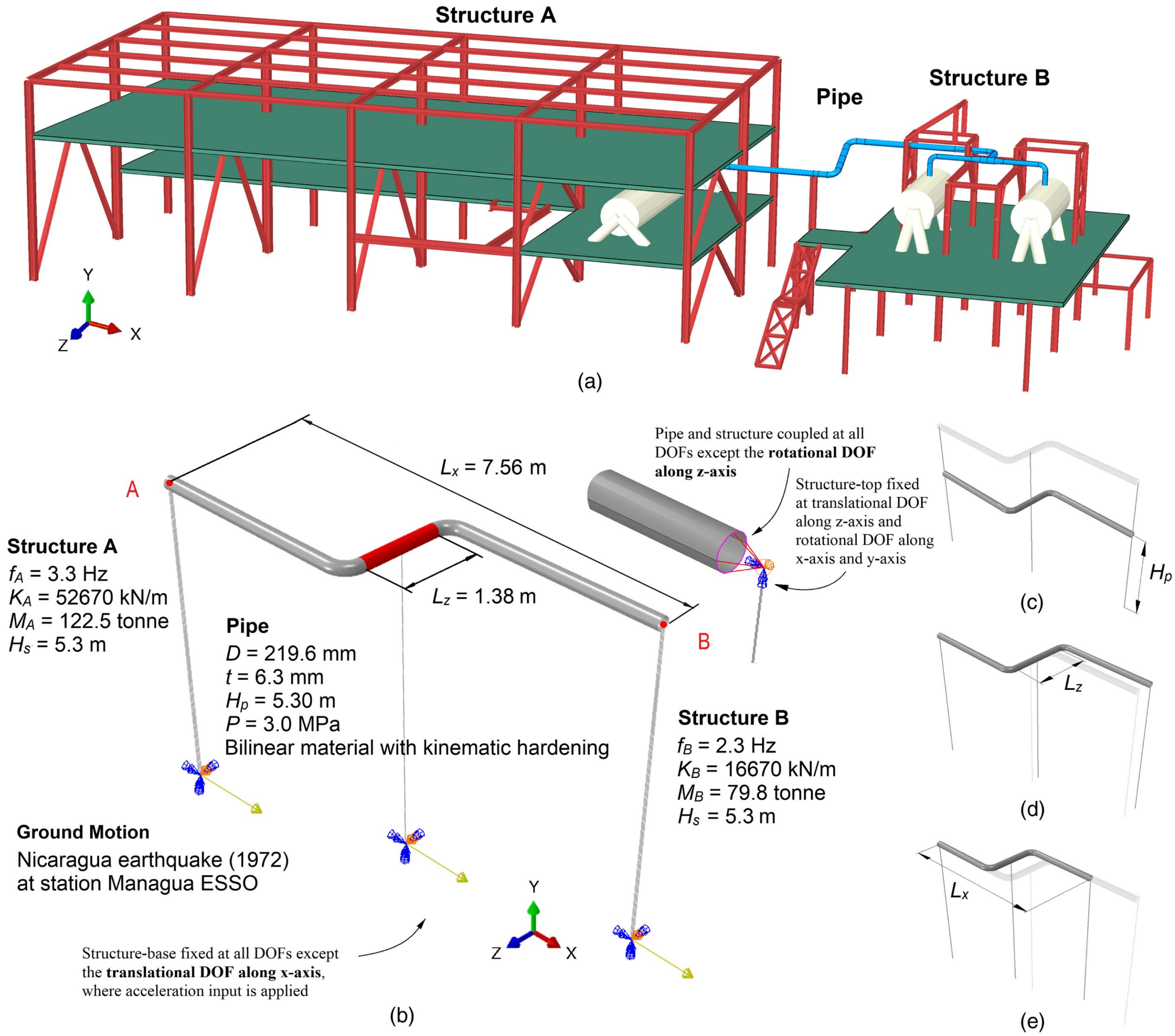

Fig. 1. Proposed structure-pipe-structure configuration: (a) detailed three-dimensional (3D) model; (b) simplified finite-element model of the reference case; (c) illustration of varying H_p; (d) illustration of varying L_z; and (e) illustration of varying L_x. DOF = degree of freedom.

a linking element between the two structures with a cross-sectional diameter of 219.6 mm, wall thickness of 6.3 mm, and two 90° elbows with bend radius of 302.0 mm located in the middle. The elbow bend factor is therefore $h = Rt/(D/2)^2 = 0.16$. The two structures are laterally separated at a perpendicular distance of 7.56 m and the length of the intermediate straight pipe segment between two 90° elbows is 1.38 m. A slender steel column supports the pipe near the middle, merely providing vertical resistance. As the overall pipe-structure system is subjected to ground excitation along the x-axis, differential displacement between the two pipe ends imposes compression or tension to the bridging pipe as the two supporting structures vibrate out-of-phase, bending the pipe elbows in-plane. This is the result of different dynamic responses of the two structures even though the earthquake ground motion they were subjected to is actually identical given their short separating distance and the common foundation and underlying soil profile.

Existing design criteria require that for the case in which a secondary system is attached to a primary system, the evaluation of the coupling effect can only be neglected if the total mass of the interacting secondary system is less than 1% of the primary supporting structure (Fouquiau et al. 2018; Taghavi and Miranda 2008). However, it has also been pointed out that if the secondary system is extended and supported at two or more locations, the coupling effect shall be investigated regardless of any mass percentage value (Firoozabad et al. 2015). The authors believe cautiousness is even more indispensable for the structure-pipe-structure configuration proposed herein, in which the secondary system (i.e., the linking NG pipe) is attached to two dynamic systems with divergent dynamic characteristics, and is therefore excited by the out-of-phase oscillation between the latter. Fundamentally, if a decoupled analysis is to be carried out for a partial structure, it is vital to ensure that the decoupling does not significantly affect the frequencies and the response of the primary system (Gupta and Tembulkar 1984). From preliminary numerical analyses of the proposed structure-pipe-structure system, it was observed that while the natural frequencies of the two structures were not altered dramatically by the presence or removal of the linking pipe element, a clear deviation of the

J. Pipeline Syst. Eng. Pract., 2021, 12(2): 04020073

structural response between the holistic case and the no-pipe case was noted; thus, coupled analysis for the proposed scenario is appropriate and necessary.

Identification of Key Problem Parameters and Maximum Pipe Demand

Analysis Outline

For an in-depth study of the problem and to find realistic conditions under which the seismic demand on the pipe becomes critical, a parametric analysis scheme was established using the general-purpose finite-element analysis software ABAQUS version 6.14. To parameterize the proposed structure-pipe-structure scenario, the two supporting structures were simplified to equivalent single-degree-of-freedom (SDOF) oscillators topped with lumped mass [Fig. 1(b)]. Due to the fact that the emphasis of the structure-pipe-structure scenario investigated herein is on the eventual damage of pipe elbows when the linking pipe element is subjected to differential displacement between its two ends, the equivalent SDOF oscillators were assumed to behave linear elastically and were modeled using the ABAQUS *Two-node Linear Beam In Space Element*, B31. The simplification preserved the elevation of the pipe anchor point, the first-mode natural frequency of the structures, the elastic swaying stiffness of the structures, and the structural mass concentrated at the elevation of gravity center of the corresponding detailed three-dimensional (3D) models. Furthermore, given that the prototypes of the two supporting structures are moment-resisting frames with axially stiff slab, which are expected to deform in shear during earthquakes, the stiff structure floors onto which the linking pipe are extended and attached are assumed parallel to the flat ground surface throughout the duration of ground excitation. Therefore, the two pipe ends in the simplified model were fixed to the oscillator at first five degrees of freedom (DOF) and were free on the sixth DOF (i.e., rotation about z-axis). Note that the simplified pipe connection may introduce a certain degree of error in terms of the state of strain on pipe, as demonstrated by Guarracino et al. (2009) both numerically and experimentally for a four-point bent pipe. It was also assumed that the ground excitation is limited to x-axis only and that the vibration of the equivalent SDOF supporting structures were restricted in the x, y-plane, which is the vibration direction of the dominant first-mode response of the corresponding detailed 3D models. Finally, we assumed that the base of the two equivalent SDOF supporting structures were fully fixed to the ground and were always subjected to the identical input ground excitation. On the other hand, the linking pipe was modeled in a greater detail to capture its potential buckling and nonlinear hysteretic response under dynamic loading. The ABAQUS *Four-node Reduced-Integration Shell Element*, S4R, was utilized for modeling the pipe geometry, assigning plastic material properties with a linear kinematic hardening rule. The mesh density on the elbows was set to 54 elements around the cylinder circumference and 3,510 shell elements in total for each 90° elbows. Coarser mesh was chosen for the straight pipe segments as the excessive strain development and nonlinearities are expected to concentrate on and around the elbows. The selected type and size of shell element have been widely used in previous pipe elbow modeling practices (Varelis et al. 2011; Vazouras et al. 2010) and were proven reliable through our preliminary analyses. To verify the model simplifications, we define $D_{diff}(t)$ as the time history of x-directional differential displacement between the two pipe ends [Eq. (1)]

$$D_{diff}(t) = u_B(t) - u_A(t) \tag{1}$$

where $u_A(t)$, $u_B(t)$ = time variation of x-axis positions of pipe-end Points A and B. Validation of the equivalent SDOF simplification in its ability of reliably reproducing the structural displacement responses was demonstrated by a comparison of $D_{diff}(t)$ results between a detailed 3D model, as shown in Fig. 1(a), and a simplified model, as shown in Fig. 1(b). The $D_{diff}(t)$ result produced by the simplified model using equivalent SDOF oscillators compared well with the corresponding $D_{diff}(t)$ obtained from detailed 3D model.

The parameters examined in the numerical parametric study are identified in Table 1. In particular, f_B/f_A is the ratio of the first-mode natural frequencies of Structures B and A, respectively. The parameter f_g is the predominant frequency of input excitation, determined at the frequency where the highest peak occurs in its fast Fourier-transform diagram. They jointly describe the fundamental dynamic mechanism of the out-of-phase oscillation between the two supporting structures. Parameter H_p aims to capture the

Table 1. List of variables examined in the parametric study

Symbol	Parameter description	Range of variation
f_B/f_A	The ratio of the natural frequencies of supporting Structures B and A	0.30 to 2.73 ($f_A \equiv 3.3$ Hz, $f_B = 1.0$ Hz to 9.0 Hz)
f_g	Predominant frequency of the input ground excitation	1.0–9.0 Hz
H_p	Elevation of pipe-end attachment points on the structures	2.0–8.0 m
K_A, K_B	Linear elastic equivalent SDOF swaying stiffnesses of the two supporting structures	50%–90% of the reference case. At 100%: $K_A = 52670$ kN/m, $K_B = 16670$ kN/m
L_z	Length of pipe between the two 90° elbows (Fig. 1)	1.5–3.0 m
L_x	Perpendicular distance between two structures (Fig. 1)	4.0–9.0 m
P	Pipe internal pressure	0–12.5 MPa
D (constant)	Pipe cross-sectional diameter	219.6 mm
t (constant)	Pipe wall thickness	6.3 mm
R (constant)	Bend radius of the 90° elbows	302.0 mm
ρ (constant)	Pipe material density	7.85 t/m^3
E (constant)	Pipe material elastic modulus	2.10×10^8 kPa
ν (constant)	Pipe material Poisson's ratio	0.3
$\sigma_{y,1}, \epsilon_{p,1}, \sigma_{y,2}, \epsilon_{p,2}$ (constant)	Pipe material bilinear nonlinarity: yield stresses and plastic strains	$\sigma_{y,1} = 275000$ kPa, $\epsilon_{p,1} = 0$; $\sigma_{y,2} = 650000$ kPa, $\epsilon_{p,2} = 0.15$
ζ (constant)	Rayleigh damping	2%
H_s (constant)	Elevation of the mass centers of the two SDOF supporting structures in simplified models	5.3 m
a_g (constant)	Peak ground acceleration (PGA) of input ground motions	1.0 g

J. Pipeline Syst. Eng. Pract., 2021, 12(2): 04020073

amplification of pipe-end differential displacement due to higher pipe elevation given the same structure, pipe, and excitation properties. The influence of pipe-structure stiffness ratio is also examined through the reflecting variable of linear elastic equivalent SDOF swaying stiffnesses of the two supporting structures K_A, K_B. The length of the straight pipe segment between the two 90° elbows L_z and the perpendicular distance between the two supporting structures L_x are further varied to assess the impact of different geometry of the structure-pipe-structure configuration. Finally, internal pressure of the NG pipe P is examined to consider the different operation conditions of a pressurized NG pipe. Other parameters, including pipe cross-sectional specifications, the geometry of the pipe elbows, pipe material properties, structural damping ratio, structure shape characterized by the elevation of its mass center, and the peak ground acceleration (PGA) of the input excitation, are taken as constants as the impacts of their variations are not unique for the problem presented herein.

The value of variables in the reference finite-element (FE) model is summarized herein as well as in Fig. 1(b). It has structural frequencies $f_A = 2.2$ Hz and $f_B = 3.3$ Hz, hence $f_B/f_A = 0.7$. The input ground motion is selected from the 1972 Nicaragua earthquake recorded at Managua ESSO station, with a predominant frequency $f_g = 2.2$ Hz (Input motion 4 in Fig. 4). The equivalent SDOF swaying stiffness of the supporting structures are $K_A = 52{,}670$ kN/m and $K_B = 16{,}670$ kN/m. Given the natural frequency and the stiffness, the mass of the two supporting structures in the reference case are $M_A = 122.5$ t and $M_B = 79.8$ t, respectively. The geometry of the structure-pipe-structure system is described with the parameters $H_p = 5.30$ m, $L_z = 1.38$ m, and $L_x = 7.56$ m. The pipe internal pressure is $P = 3.0$ MPa. Note that in each of the following variations in the parametric study, only the examined parameter(s) will be deviated from the reference case in each section.

Structural and pipe response quantities examined throughout the parametric study are $D_{diff,max}$ and $\epsilon_{h,max}$. The peak differential displacement between two pipe ends, $D_{diff,max}$, is defined as the absolute value of the largest in time pipe-end differential displacement $D_{diff}(t)$ that occurred during the excitation

$$D_{diff,max} = max(|D_{diff}(t)|), \quad t = 0 \rightarrow t_g \tag{2}$$

where t_g = total length of the input ground excitation. $D_{diff,max}$ is therefore a nonnegative scalar derived for each analysis case, providing insight into the level of global response of the coupled structure-pipe-structure dynamic system. Similarly, the maximum hoop strain on the elbows, $\epsilon_{h,max}$, defined as the largest amplitude of elbow hoop strain $\epsilon_h(t)$ obtained during the excitation within the 90° bent elbows, represents the level of local seismic elbow strain demand. Like any peak values, the $D_{diff,max}$ and the $\epsilon_{h,max}$ neither reflect the time variation nor the potential cumulative character of the response quantities. Nonetheless, as scalars, they provide straightforward indications of the level of seismic demand to the pipe and can be comprehended within the context of parametric study.

Effect of Structural and Ground Motion Frequencies

To gain understanding into the frequency-dependency of the peak differential displacement between two pipe ends $D_{diff,max}$ and the induced maximum elbow hoop strain $\epsilon_{h,max}$, we examine the ratio of first-mode natural frequencies of the two supporting structures f_B/f_A and the frequency content of the input excitation characterized by its predominant frequency f_g. Given that the purpose of the study was not to explore fatigue or ground motion duration impact on nonlinear response of the elbows, but to identify the effect of ground motion frequency content on the developed hoop strains, wavelet pulses were employed for analysis having an amplitude of 1.0 g and a predominant frequency f_g varying from 1.0 Hz to 9.0 Hz. More precisely, Ricker wavelets (Ricker 1943) were used to excite a series of models with varying structural frequency ratio f_B/f_A ranging from 0.30 to 2.73 (corresponding to a variation of f_B ranging from 1.0 Hz to 9.0 Hz while f_A was kept equivalent to 3.3 Hz), representing the pulse-like waveforms of acceleration inputs with a narrow frequency bandwidth (Fig. 2).

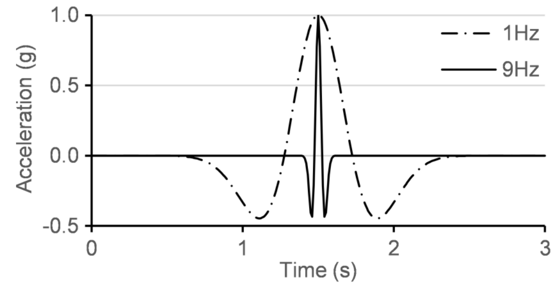

Fig. 2. Illustration of acceleration time histories of Ricker wavelets with varying predominant frequencies.

Inspection of $D_{diff,max}$ [Fig. 3(a)] and $\epsilon_{h,max}$ [Fig. 3(b)] results over the variation of structural frequency ratio f_B/f_A reveals nonzero responses in all cases except when $f_B/f_A = 1.0$. For these cases, a minimum $D_{diff,max}$ response of around 25 mm and a minimum $\epsilon_{h,max}$ response of around 0.1% exist even when none of the structure natural frequencies f_A and f_B are close to the predominant frequency of excitation f_g. This indicates that the out-of-phase oscillation between two supporting structures can occur as long as their first-mode natural frequencies of vibration are not identical. On the pipe elbows, hoop strain develops accordingly during the excitation as the elbows bend due to the differential motion exerted between the two pipe ends.

Inspection of $D_{diff,max}$ and $\epsilon_{h,max}$ results over the variation of input predominant frequency f_g shows the fact that the responses will reach local maximum values when resonance to the input excitation occurs for at least one of the supporting structures. For all models with a f_B/f_A value other than 1.0, wavelet excitation with predominant frequencies $f_g = 3.0$ Hz and $f_g = 3.5$ Hz have led to $D_{diff,max}$ response greater than 58 mm and $\epsilon_{h,max}$ response higher than 0.51%, which can be attributed to the resonance of Structure A (whose natural frequency $f_A \equiv 3.3$ Hz) to these inputs. We note that the responses observed in these cases are nearly constant as long as Structure A is the only resonant supporting structure. A series of peaks goes diagonal across the 3D plots [i.e., from the point ($f_g = 1.0$ Hz, $f_B/f_A = 0.3$) to the point ($f_g = 9.0$ Hz, $f_B/f_A = 2.73$)] reflect the resonance of Structure B (whose natural frequency f_B varies between 1.0 Hz and 9.0 Hz) to the corresponding wavelet excitation. These diagonal peaks are higher as the natural frequency of Structure B f_B and the predominant frequency of excitation f_g are lower. Moreover, we notice that the $D_{diff,max}$ and the $\epsilon_{h,max}$ responses further amplify when the natural frequencies of the two supporting structures, f_A and f_B, are both close to the predominant frequency of excitation f_g. Within the scheme of this parametric study, the phenomenon is observed at the analysis case $f_g = 3.0$ Hz and $f_B/f_A = 0.92$ (i.e., $f_A \equiv 3.3$ Hz, $f_B = 3.04$ Hz), which results in $D_{diff,max} = 120$ mm and $\epsilon_{h,max} = 0.78\%$. Notice that this $D_{diff,max}$ value is almost exactly twice as much as the $D_{diff,max}$ values observed in cases in which Structure A is the sole supporting structure in resonance with the $f_g = 3.0$ Hz wavelet input, whereas the $\epsilon_{h,max}$ value is intensified by around 50%.

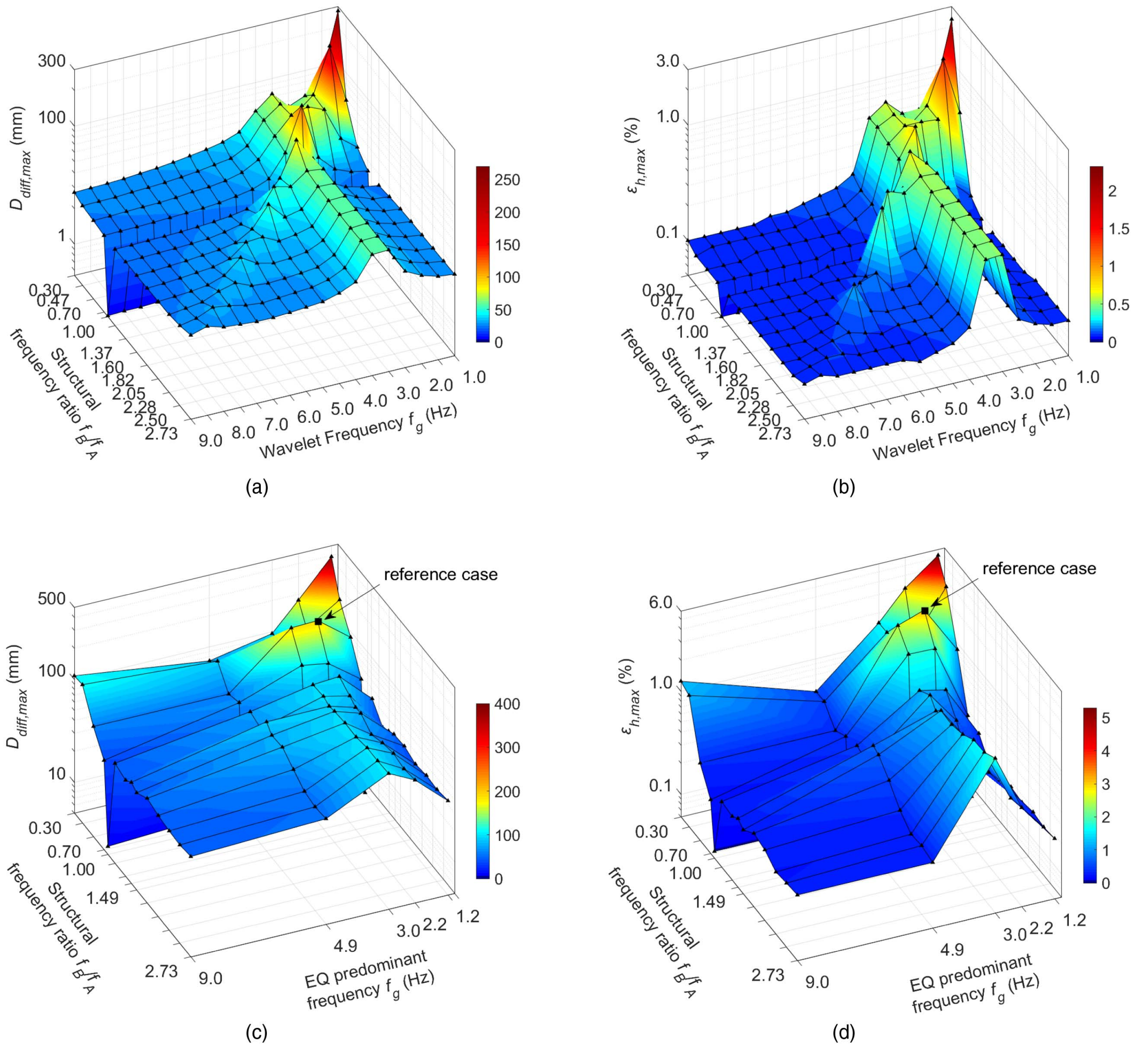

Fig. 3. $D_{diff,max}$ and $\epsilon_{h,max}$ responses with respect to variations of structural frequency ratio f_B/f_A and predominant frequency of excitation f_g: (a and b) Ricker wavelets; and (c and d) earthquake ground motions. Note the variation of f_B/f_A from 0.30 to 2.73 corresponds to $f_A \equiv 3.3$ Hz and f_B varying from 1.0 to 9.0 Hz.

Looking through all analysis cases, the global maximum values of $D_{diff,max}$ and $\epsilon_{h,max}$ occur at the analysis case $f_g = 1.0$ Hz and $f_B/f_A = 0.30$ (i.e., $f_A \equiv 3.3$ Hz, $f_B = 1.0$ Hz), resulting in $D_{diff,max} = 274$ mm and $\epsilon_{h,max} = 2.32\%$. The aforementioned observations indicate that a combination of supporting structures with low first-mode natural frequencies (either a single or both supporting structures) and ground excitation with a low predominant frequency can lead to the onset of higher out-of-phase vibrations between the two supporting structures, hence a higher seismic elbow strain demand.

Of course, real earthquake ground motions are typically rich in a broader range of frequency contents. A selection of five earthquake accelerograms with different predominant frequencies (Table 2 and Fig. 4) and their PGA scaled to $a_g = 1.0$ g were used to excite the FE models with varying f_B/f_A values. Note that the intention of this practice was not to extensively explore the impact of different ground motions to the proposed structure-pipe-structure scenario but to provide a proof that the observations gained from the wavelet cases are also conceptually applicable for real ground motions. While similar trends can be qualitatively confirmed by interpreting Figs. 3(c and d), $D_{diff,max}$ and $\epsilon_{h,max}$ values obtained using ground motion inputs carry greater randomness. Overall, a higher magnitude of responses can be observed due to the much-longer duration of excitation, in which global maximum values $D_{diff,max} = 391$ mm and $\epsilon_{h,max} = 5.26\%$ are indicated at the analysis case $f_g = 1.2$ Hz (i.e., Input motion 5), $f_B/f_A = 0.30$ (i.e., $f_A = 3.3$ Hz, $f_B = 1.0$ Hz). The reference case of the parametric study, $f_g = 2.2$ Hz (i.e., Input motion 4) and

Table 2. List of earthquake records used as input ground motions

Identifier	Event	Station and recorded direction	Unscaled PGA (g)	Predominant frequency f_g (Hz)
1	San Fernando (1971)	Santa Felita Dam (Outlet), 262	0.15	9.0
2	Northridge (1994)	Lake Hughes #9, 90	0.26	4.9
3	San Fernando (1971)	Castaic - Old Ridge Route, 21	0.32	3.0
4	Nicaragua (1972)	Managua ESSO, 90	0.26	2.2
5	San Fernando (1971)	Palmdale Fire Station, 120	0.11	1.2

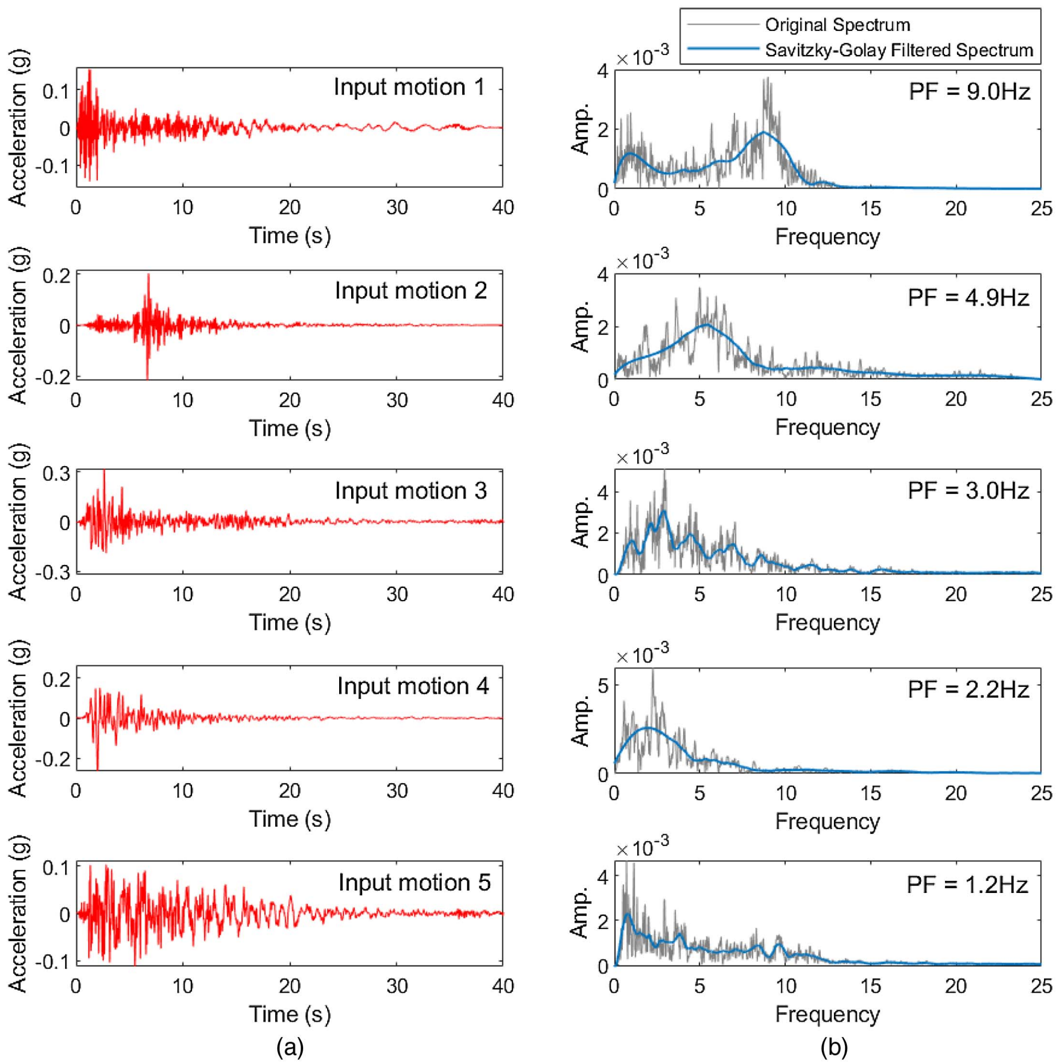

Fig. 4. Acceleration time histories (a) and their fast Fourier-transform amplitudes; and (b) used as input ground motions. PF = predominant frequency.

$f_B/f_A = 0.70$ (i.e., $f_A = 3.3$ Hz, $f_B = 2.3$ Hz), which is also the case later tested in HS, is marked on the figures where $D_{diff,max} = 189$ mm and $\epsilon_{h,max} = 3.13\%$ are predicted.

Effect of the Pipe-End Attachment Point Elevation

Given the same NG pipe, the same structural dynamic properties, and the same ground motion input, the dynamic response of the structure-pipe-structure system can be different depending on the specific location; in particular, the elevation of the attachment points where the two ends of the linking pipe element are connected to the supporting structures. In the parametric study, the two pipe-end attachment points have identical elevation and their variations are assumed simultaneous so that a single parameter (i.e., pipe-end attachment elevation H_p) is sufficient for describing the phenomenon. A reasonable variation of H_p in the range of 2.0–8.0 m was considered to account for NG pipes connected at different heights between two typical industrial structures in NG plants. Note that because the two supporting structures are represented by equivalent SDOF oscillators, the simplified FE models have the limitation in replicating the true profile of structural lateral deformation along their elevation during the excitation. This means the analysis accuracy reduces when the pipe-end attachment elevation H_p is far off from the elevation of mass centers of the SDOF supporting structures H_s, which is equivalent to 5.3 m. Nevertheless, the impact of varying H_p to the global and local system responses can be reflected.

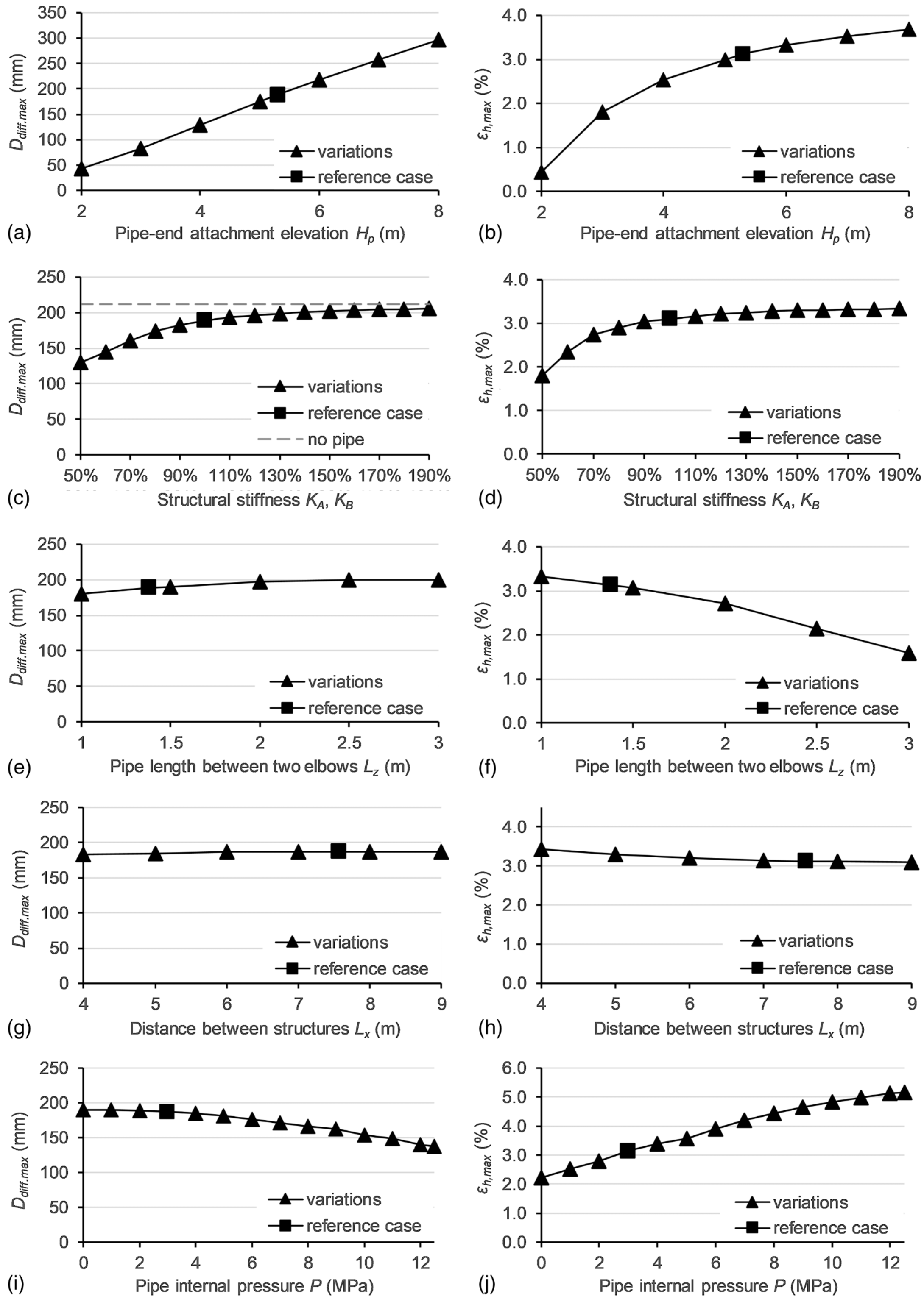

Fig. 5. $D_{diff,max}$ and $\epsilon_{h,max}$ responses with respect to variations of H_p, K_A and K_B, L_z, L_x, as well as P.

Within the range of examined pipe-end attachment elevation H_p values, analysis result shows an linearly correlated relationship between the H_p and the $D_{diff,max}$ response [Fig. 5(a)]. The $D_{diff,max}$ maxes out at 296 mm and reaches its minimum of 43 mm when the pipe-end attachment elevation is $H_p = 8.0$ m and $H_p = 2.0$ m, respectively. On the other hand, while the $\epsilon_{h,max}$ response [Fig. 5(b)] also becomes larger as the H_p is larger, the correlation is not linear. Compared to the reference case in which $H_p = 5.3$ m, increasing the H_p value by 2 m intensifies the $\epsilon_{h,max}$ output by no more than 16%, whereas decreasing the H_p value by the same amount results in around 40% of reduction on the $\epsilon_{h,max}$ response.

Effect of the Structural Stiffness

An important property of the coupled structure-pipe-structure system is characterized by the relative ratio between the stiffness of the linking pipe element and those of the supporting structures. Considering the fact that a total of two structures are involved in the scenario with different swaying stiffness values and the nonlinear behavior expected for the linking pipe element, we herein examine only the variation of the linear elastic equivalent SDOF structural stiffness and use it to conceptualize the variation of pipe-structure stiffness ratio, instead of defining the ratio explicitly. A higher input of structural stiffness indicates a lower pipe-structure stiffness ratio and vice versa. In the parametric study, the stiffness of the two structures, K_A, K_B, are assumed to vary simultaneously so that their values in different analysis cases can be expressed using a single percentage value with regard to the reference model. To give an idea, the linear elastic equivalent SDOF swaying stiffnesses of Structure A and Structure B in the reference case are $K_A = 52670$ kN/m and $K_B = 16670$ kN/m, while the x-axis initial stiffness of the linking pipe element is equivalent to 751.5 kN/m. Additionally, in order to reflect the case when pipe-structure stiffness ratio is zero, we also analyzed the aforementioned models with the linking pipe element being removed. Note that the variation of K_A, K_B is always accompanied by a corresponding change of equivalent SDOF masses of the two structures, so that the natural frequencies of the two supporting structures are kept invariant in this section.

The $D_{diff,max}$ [Fig. 5(c)] and $\epsilon_{h,max}$ [Fig. 5(d)] responses are plotted against structure stiffness K_A, K_B. The $D_{diff,max}$ response is higher for cases when structural stiffness is higher (i.e., lower pipe-structure stiffness ratio), indicating a weakened coupling effect between the two supporting structures introduced by the weaker linking pipe element. Also, we observe constant numerical outputs of $D_{diff,max} = 212$ mm for all analysis cases when the linking pipe element is removed, represented by the dotted line on Fig. 5(c). The $D_{diff,max}$ curve continually approaches the dotted line but does not meet it within the range of examined K_A, K_B. One might perceive that the curve and the dotted line will never meet at any finite value of structural stiffness as long as the linking pipe element keeps its presence, hence its stiffness. A similar trend applies to the $\epsilon_{h,max}$ response as well. As the structure-pipe-structure interaction is weakened due to a higher K_A, K_B input, the elbow strain demand correspondingly raises and approaches a theoretical maximum value as the pipe-structure stiffness ratio approaches zero. For the proposed structure-pipe-structure configuration, the $D_{diff,max}$ result exceeds 95% of the no-pipe cases when structural stiffness percentage exceeds 180% of the reference model, in which case $K_A = 105340$ kN/m and $K_B = 33330$ kN/m. In such a case when the pipe-structure stiffness ratio is lower than a certain level, hence the $D_{diff,max}$ response does not clearly deviate from the corresponding no-pipe case, a coupled analysis is rendered unnecessary. This means predetermined structural responses from a no-pipe case can be used as inputs to predict seismic demand of the linking pipe element with acceptable accuracy. However, we stress that a coupled analysis is always recommended in the preliminary stage of any pipe-related research in which similar structure-pipe-structure configurations are involved, so that the boundary condition of the pipe can be made realistic. Additionally, when deciding whether a coupled analysis can be neglected, it would be good practice to inspect not only the peak value $D_{diff,max}$ but the quantity's full time variation $D_{diff}(t)$ when possible.

Effect of the Straight Pipe Length between Two Elbows and the Perpendicular Distance between Two Supporting Structures

The length of the straight pipe segment between the two 90° elbows L_z and the perpendicular distance between the two supporting structures L_x are variables describing the different geometry layouts of the linking pipe element. The examined range of L_z was selected as 1.0–3.0 m and the range of L_x was selected as 4.0–9.0 m. Within these ranges the overall length and shape of the linking pipe element is realistic for typical bridging pipes within NG plants, while further complicating the parametric study by adding a pipe rack is avoided. The two 90° elbows are assumed to always locate exactly at the middle, forming the linking pipe element in a symmetrical shape.

The $D_{diff,max}$ response are found to have a very weak dependency on the variation of L_z [Fig. 5(e)] as the deviation of responses between all cases are less than 10%. On the other hand, the $\epsilon_{h,max}$ response reduces significantly as the L_z is larger [Fig. 5(f)], there is a 50% reduction on elbow strain demand as the L_z increases from the reference case of 3.0 m. The similar global displacement responses of the structures with respect to different L_z inputs is because the x-axis stiffness of the linking pipe element remains almost unchanged within the range of L_z variation. Meanwhile, a shortened L_z means that the elbows are subjected to a larger bending angle, hence a much higher local elbow strain demand. On the other hand, the variation of L_x has led to almost constant $D_{diff,max}$ [Fig. 5(g)] and $\epsilon_{h,max}$ [Fig. 5(h)] responses, in which the deviation between all cases is less than 3% and 10%, respectively.

Effect of Pipe Internal Pressure

NG is usually highly compressed for its transmission through pipes. In the parametric study, pipe internal pressure P in the range from zero to 80% of the reference pipe's nominal yield stress, $80\% p_y = 80\%(2\sigma_{y,1}t/D) \approx 12.5$ MPa, was examined. Note that the uniqueness of variable P from the rest of the variables examined in the parametric study is that the internal pressure affects both the demand and the capacity of the pipe. The collapse moment of pipe elbows is known to increase with higher internal pressure up to a certain threshold value, and then decrease with further increasing of internal pressure. Previous research showed that for the 90° elbows with bend factor $h \approx 0.16$, this threshold value is around $P = 10.5$ MPa when the elbows are subjected to closing bending moment (Shalaby and Younan 1998).

The peak differential displacement between two pipe ends $D_{diff,max}$ is lower as a result of higher P input [Fig. 5(i)]. This is because an increased pipe internal pressure can lead to higher x-axis stiffness of the linking pipe element, hence a more pronounced structure-pipe-structure interaction to mitigate the differential displacements between two supporting structures. However, although the $D_{diff,max}$ response tends to reduce with higher P so that effectively the 90° elbows are less bent during the excitation, its benefit to the alleviation of seismic elbow strain demand is completely suppressed by the presence of the higher pipe internal pressure itself. The maximum elbow hoop strain $\epsilon_{h,max}$ soars as the P input increases [Fig. 5(j)].

Experimental Setup: Hybrid Simulation

System Substructuring Scheme

Considering the nonnegligible structure-pipe-structure interaction and the size of the interactive industrial structures, HS is believed a necessary and efficient way for experimentally investigating the buckling potential and the detailed nonlinear hysteretic behavior of the linking pipe element as well as the interactive response of the overall system. We developed a HS scheme based on the reference model used in the parametric study, in which a physical specimen of the linking pipe element, consisting of three straight pipe

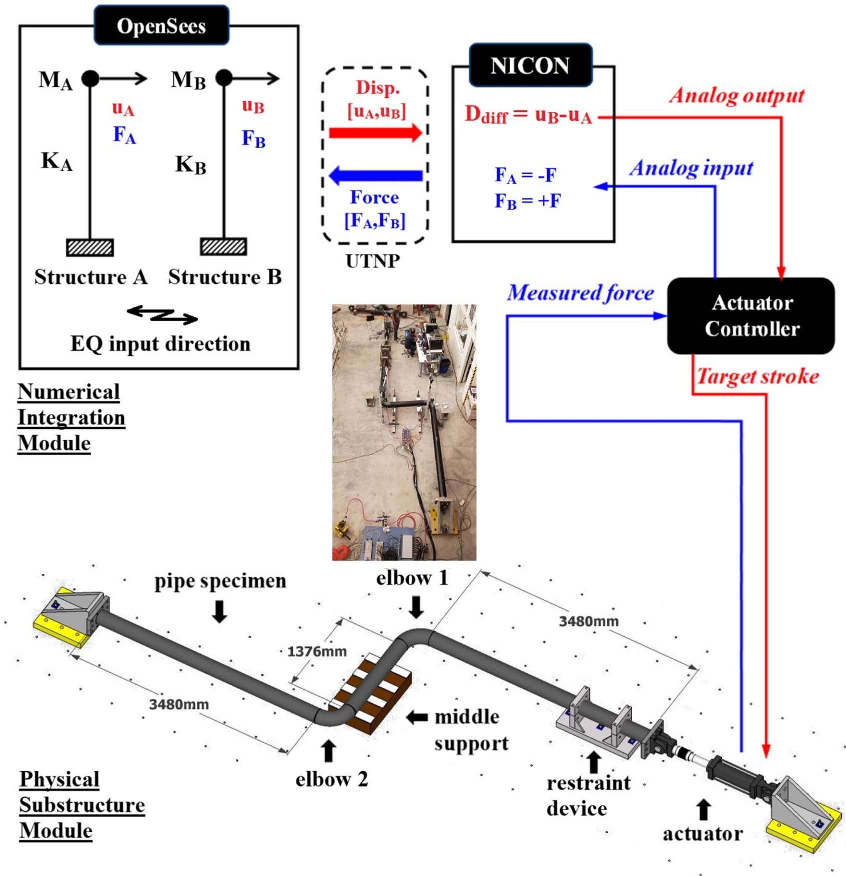

Fig. 6. Substructuring scheme and key components of the HS. NICON = network interface for the controller; UTNP = University of Toronto networking protocol; and EQ = earthquake.

segments and two 90° elbows, was tested at the Structures Laboratory of the University of Patras, Greece, whereas the complementary part involving the two supporting structures was solved numerically (Park et al., forthcoming). A total of two substructure modules, as illustrated in Fig. 6 and that will be discussed in the following sections, were therefore configured for the HS in order to investigate the coupled response of the structure-pipe-structure system.

The generalized HS framework, UT-SIM (second edition), developed by the University of Toronto research group (Huang and Kwon 2018; Mortazavi et al. 2017), was used for integrating the numerical and experimental substructures. The UT-SIM framework employs the University of Toronto Networking Protocol (UTNP) for communication while a software library provides useful functions in exchanging data between diverse numerical and experimental models. The generalized nature of UT-SIM framework assigns each substructure module with an interface of communication. In this HS scheme, OpenSees computational platform version 2.4.3 (rev 5645) (Mazzoni et al. 2006) was selected to perform the analysis tasks of solving both the numerical substructure and the main integration algorithm. Therefore, an OpenSees user defined element termed *SubStructure* was featured to the numerical model to collect the required restoring force through UTNP. On the other hand, a software called the network interface for the controller (NICON) (Zhan and Kwon 2015), based on the *LabView* programming environment and *National Instrument* hardware, allows communication, coordinate conversion, analog voltage generation, data transmission, and acquisition of the physical substructure module.

During the entire HS, the numerical integration algorithm calculates a set of command displacements (u_A, u_B) at each analysis time step. This digital information is passed from the numerical integration module to the physical substructure module via the UTNP-utilizing communication interfaces featured in the UT-SIM framework, consisting of the *SubStructure* OpenSees element for the former and the NICON software for the latter. The calculated structural displacements are received by the NICON and go through a simple calculation which turns them into the differential displacement to be imposed to the physical pipe specimen [$D_{diff}(t) = u_A(t) - u_B(t)$], before the command is then converted into an analog voltage signal employing *National Instrument* data acquisition digital-to-analog conversion hardware. The generated displacement command is subsequently interpreted by a modular actuator controller unit, which drives the unidirectional hydraulic actuator using proportional–integral–derivative (PID) control. Given an accurate actuation control and the fact that strain rate effect due to seismic motion is believed to have little influence on the material stress-strain behavior of pipe (Yoshizaki et al. 2000), the overall structure-pipe-structure system is subjected to deformations and damage equal to those a real earthquake would generate. The structural response parameters (actuator force and actually imposed displacement) are not known in advance and are measured and recorded during the HS via the actuator load cell (243.45 Actuator, MTS Systems, Eden Prairie, Minnesota) and a high-resolution Temposonics transducer (MTS Systems, Eden Prairie, Minnesota) attached on the actuator. The restoring force and displacement responses of the physical substructure acquired at the current time step are converted to digital form and fed back to the numerical integration algorithm. Eventually the current time step is completed and HS progresses to the next one until full completion of the excitation record.

Numerical Integration Module

The numerical integration module of the proposed HS scheme contains the FE model representing the two supporting structures in the proposed structure-pipe-structure scenario and handles the main integration algorithm for dynamic time history analysis. The linear elastic equivalent SDOF modeling approach used in the parametric study for the two supporting structures was transplant to the HS in the OpenSees numerical integration module. By employing the modeling approach and applying the identical assumptions and boundary conditions to the numerical substructure, we ensure the compatibility and equilibrium condition at the numerical-physical coupling DOF (i.e., x-axis differential motion between the two pipe ends) so that a single unidirectional actuator is sufficient for applying the appropriate boundary condition to the physical substructure module during HS. Note that in the OpenSees model, the equivalent SDOF columns were modeled using the *Elastic Timoshenko Beam-Column Element*, which employs the same beam theory as the ABAQUS B31 element used in the parametric study models. A dedicated *SubStructure* element was defined, acting as the interface of communication for the numerical substructure. Furthermore, supporting structure properties employed in the numerical integration module were identical to those of the reference case in the parametric study. Structure A had a natural frequency of $f_A = 3.3$ Hz and mass of $M_A = 122.5$ t; Structure B had a natural frequency of $f_B = 2.3$ Hz and mass of $M_B = 79.8$ t. The numerical model was assigned with 2% Rayleigh damping and alpha-operator splitting method (Combescure and Pegon 1997) was used as the integration algorithm. The total analysis period of the HS was set to 10 s, corresponding to a total of 1,000 time steps as the step size was selected to be 0.01 s. The first 7 s of the accelerogram from the 1972 Nicaragua Earthquake recorded at the Managua ESSO station (i.e., Input motion 4 as shown in Fig. 4), with a predominant frequency of 2.2 Hz and the PGA scaled to 1.0 g, was used as the input ground motion to the numerical integration module in HS.

The effectiveness of the numerical integration module was verified by a series of OpenSees-ABAQUS multiplatform simulations prior to the actual HS, in which the physical substructure module containing the linking pipe specimen was represented by an ABAQUS numerical replacement. Accuracy and stability of the integration process, effectiveness of the OpenSees numerical model, and the smooth operation of the associated UT-SIM framework components which cooperate with the numerical substructure were double-checked.

Physical Substructure Module

The physical substructure module is composed of the full-scale physical specimen of the linking NG pipe and relevant accessories including a hydraulic actuator, an actuator controller, the HS interface software NICON that links the actuator controller to the numerical model, the measuring instruments, and a data acquisition system.

The physical NG pipe specimen residing at the Structures Laboratory of the University of Patras, Greece (Fig. 6), includes three straight pipe segments welded in situ on two 90° elbows with a cross-sectional diameter (D) of 219.6 mm and a pipe wall thickness (t) of 6.3 mm. The length of the straight pipe segment located between the two elbows (L_z) is 1.38 m, the length of the other two straight pipe segments is 3.48 m and the bend radius of the 90° elbows (R) equals 302.0 mm. Therefore, the perpendicular distance between the two structures (L_x) is 7.56 m, the pipe nondimensional geometry parameters are $R/D = 1.38$, $D/t = 34.86$ and the elbow bend factor is $h = Rt/(D/2)^2 = 0.16$. Before the HS, a water pumping system applied pipe internal pressure (P) of 3.0 MPa to the pipe specimen, accounting for the compressed NG inside the pipe. In the laboratory, the pipe specimen was rigidly clamped onto the strong laboratory floor through a triangular connector at one end, while its other end was attached to a unidirectional actuator. A low-friction guiding device was set up around the straight pipe segment near the actuator side, limiting the actuator's movement along the x-axis. This was to ensure the SDOF equilibrium condition at the numerical-physical coupling node so that the errors introduced at the interface between two HS substructures were minimized. On the other hand, because the pipe specimen was in contact with the guiding device, a contact force with unknown magnitude was inevitably included as part of the specimen restoring force since potential horizontal or vertical pipe inclination might occur during the HS. As a result, a small error may still exist in the force feedback to the numerical integration module at every analysis time step, which could harm the accuracy of HS result. While all contacting surfaces between the pipe and the guiding device were covered with polytetrafluorethylene sheets and were highly lubricated to reduce friction, the upper-half of the guiding device was also left rather loose to further reduce the impact of contact/pipe inclination to its minimum. Two strip supports with polytetrafluorethylene and lubricated flat surfaces were placed under the middle of the pipe specimen to provide pipe constraint in the vertically downward direction, simulating the single-column pipe support in the proposed structure-pipe-structure configuration. By doing so, initial pipe flexure due to its self-weight was prevented.

The effectiveness of the laboratory setup was validated to ensure that the presence of the auxiliary gears do not obstruct the validity of our model assumptions. Evidence obtained during and after preliminary nondamaging HS showed a minor effect of the contacting force originated from the restraint device and the strip supports. We noted that the pipe specimen started to deform elastically at a very small applied actuator displacement, indicating a very small unwanted contacting force in the laboratory setup. The force is experimentally estimated at less than 2% of the maximum restoring force that the linking pipe specimen would experience during the full-amplitude HS. Given the previous discussion, it is concluded that experimental results obtained from the HS laboratory setup are valid.

Still, if not tuned properly, the HS setup can generate erroneous results for various other reasons. These may include the working frequencies and amplitudes of the physical setup, the condition of the tested specimen, the actuator, the control device, the type of chosen control algorithm and its parameter setting, as well as the selected size of the ramp and hold periods for each analysis time step (Molina et al. 2011). Hence, the effectiveness of the physical substructure module was further optimized and verified by a series of nondestructive HS prior to the actual HS. Firstly, through trial and error, appropriate parameters of the PID controller as well as the allowable velocity of the actuator were determined so as to confront the noise in the reference (analog) signal due to analog-to-digital (A/D) conversion and to minimize control error. By the same token, low actuator responsiveness yields the need for longer stabilization period at the end of the ramp and an appreciable hold period for averaging an adequate number of restoring force sample values (analog). As a result, testing wall-clock time increased considerably. In the trade-off between HS accuracy and time efficiency, an appropriate maximum actuator speed was selected equal to 1 mm/s, and a waiting period of 5 s was used after each execution of command displacement so as to reduce the undesirable fluctuation of forces. An averaged measurement of reaction force was designed to be taken in a period of 2 s after the 5-s waiting period, so that the noise-to-signal ratio in the measurement can be further reduced. Such a configuration ensures the numerical integration module to get representative force and displacement feedback from the physical substructure module, while producing a relatively reasonable 6-h HS execution time. Moreover, the initial stiffness of the physical NG pipe specimen, which is required as an input variable for the alpha-operator splitting numerical integration algorithm, was experimentally measured.

Instrumentation

Strain Gauges

A 16-channel data acquisition system for strain measurement was used for the test. The strain gauges were installed as shown in Fig. 7(a). The four locations with significant strains on a half-elbow were identified based on numerical analyses. Because of the possible out-of-plane deformation of the pipe and the existence of the restraint device, the pipe specimen may behave unsymmetrically despite its symmetrical geometry. Thus, all four half-elbows were instrumented with strain gauges at the same locations to ensure the measurement of maximum strains on the elbows.

Ovalization Measuring Devices

Two special-purpose ovalization measuring devices (one per elbow) with LVDTs were used in order to measure the development of cross-sectional ovalization on the elbows [Fig. 7(b)]. The main body of the ovalization measurement device is a light steel frame that is in contact with the elbow at four points along the perimeter of a single cross section; the frame is welded to the elbow at its intrados, while displacement measurements are taken at the elbow's extrados and two flanks. The steel frame itself is considered rigid, allowing the LVDTs to be pressed against the elbow wall, thus obtaining the correct measurement of elbow cross-sectional diameter change, or *flattening* (Varelis et al. 2012), at two perpendicular pipe diameters. The devices are installed in the middle (45°) section of the elbows, where maximum elbow flattening was predicted. Preliminary numerical analysis also proofed a negligible impact to the pipe responses brought by the welded ovalization devices.

Observations and Results from Hybrid Simulation

The examined linking NG pipe element showed a favorable performance under the specific structure-pipe-structure configuration and the input earthquake ground motion, during which no leakage was observed. The HS confirmed the minor influence of the contacting force originated from the auxiliary restraint device and the strip supports, and no out-of-plane deformation of the pipe specimen was observed during the HS.

Differential Displacement Time History and Force-Displacement Relationship

Time history of differential displacement between the two pipe ends, $D_{diff}(t)$, and force-displacement relationship of the linking NG pipe (Fig. 8) obtained from the HS (*HS holistic*) and its corresponding numerical model in ABAQUS (*FEA holistic*) are compared to gain insight into the hysteretic response of the linking pipeline element. The $D_{diff}(t)$ response represents the system response on a global level, whereas the force-displacement curve reveals evident hysteresis behavior of the pipe. The $D_{diff}(t)$ response of the HS is very similar to its finite-element analysis (FEA) counterpart in the first-half of the ground motion, leading to identical peak differential displacement between two pipe ends at $D_{diff,max} = 189$ mm. As the input excitation gradually dies down, more discrepancy between the two curves are observed. It is also noted that while the FEA holistic model of the structure-pipe-structure system predicted well the amplitude of relative displacement time history, the result obtained from HS showed a slightly higher vibration frequency. Additionally, the $D_{diff}(t)$ response of standalone structures without being coupled by the linking pipe element (*FEA no pipe*) is presented, showing the impact of structure-pipe-structure interaction.

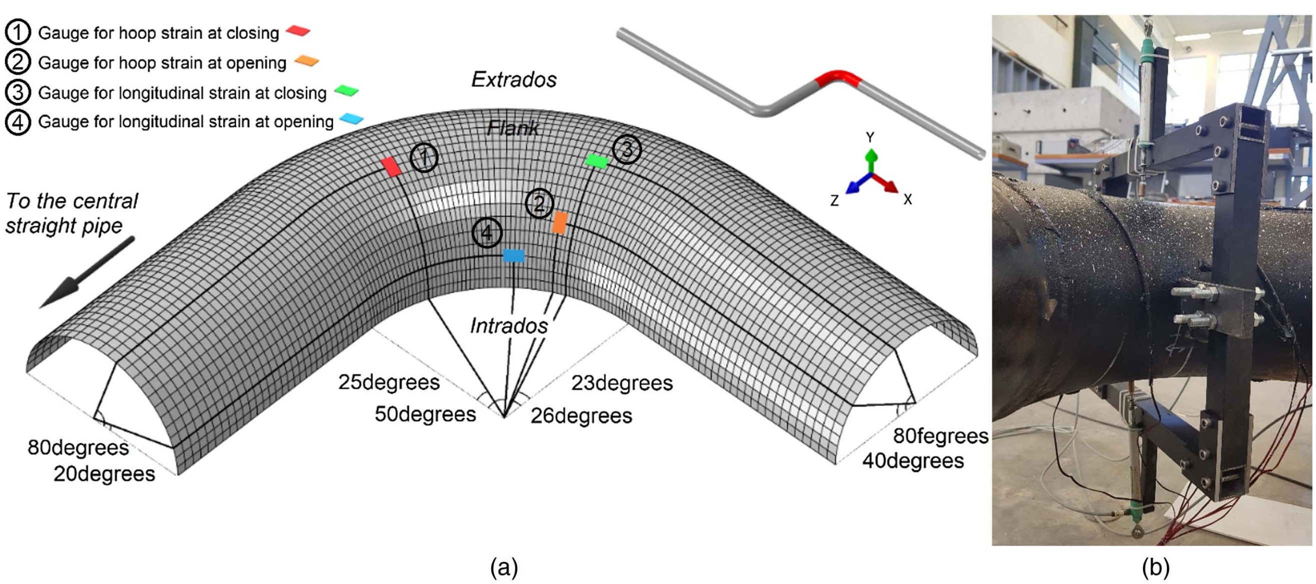

Fig. 7. Instrumentation: (a) strain gauges; and (b) ovalization device.

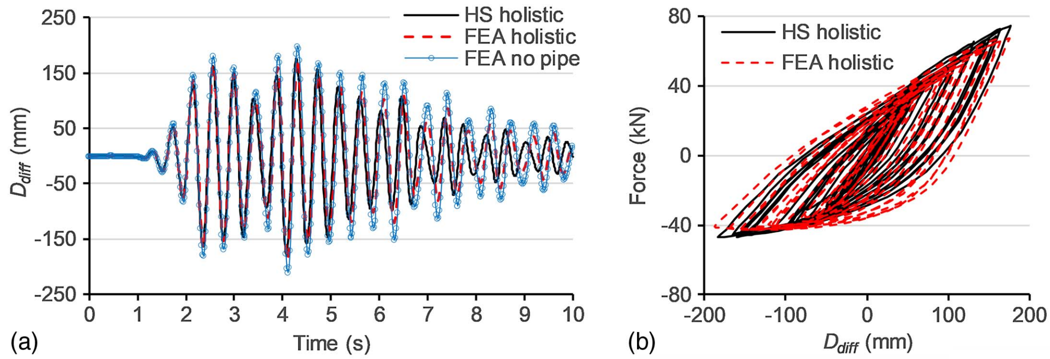

Fig. 8. (a) $D_{diff}(t)$ responses; and (b) force-displacement curves obtained from the HS and the corresponding FE prediction. The $D_{diff}(t)$ response of a no-pipe case is also plotted to reflect the impact of structure-pipe-structure interaction.

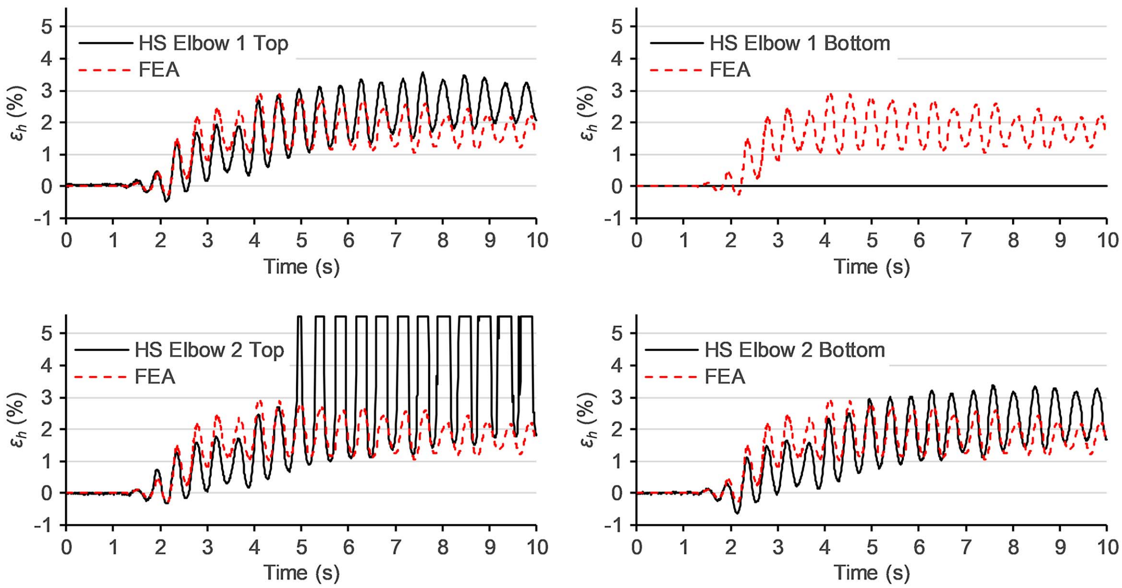

Fig. 9. $\epsilon_h(t)$ responses on four half-elbows of the HS and the corresponding FE prediction, obtained at the significant strain location where maximum hoop strain occurred in FE prediction.

Strains on Elbows

Four groups of strains were monitored at the top and bottom surfaces of the two elbows to account for the possible unsymmetrical behavior of the pipe specimen during the HS due to the presence of the constraint device. Despite this concern, test results were found to be similar on the two elbows. Critical hoop strain measurement from the HS, $\epsilon_h(t)$, sampled physically at the locations corresponding to where the maximum elbow hoop strain was observed in numerical predictions, is plotted in Fig. 9. We note that measurement on the bottom side of Elbow 1 shows zero strain and the measurement on the top side of Elbow 2 saturates after 5 s into the HS. These errors can be attributed to a detached or a damaged gauge. Ratcheting effect of strain development is clear from both HS results and FE prediction. The maximum elbow hoop strain during the HS occurred on the top side of Elbow 1 (i.e., the one close to the actuator) at $\epsilon_{h,max} = 3.49\%$, whereas the FE predicts $\epsilon_{h,max} = 3.13\%$. Moreover, the ratchet effect of elbow hoop strain development recorded during the HS was only approximately captured by FEA, in which the time spot when $\epsilon_{h,max}$ occurs and the general trend of strain development was quite different.

Cross-Sectional Ovalization

Cross-sectional ovalization is quantified and visualized in the form of cross-sectional flattening, i.e., the change of elbow diameter in a certain direction [Fig. 10(a)]. The horizontal and vertical cross-sectional flattening on both elbows were compared against the numerical prediction. The hybrid simulation result shows a less significant permanent cross-sectional flattening at the vertical direction when compared to the numerical prediction: at around 2.5–3.5 s on the time history, the center line of the *FEA-vertical* curve shifted upward with a magnitude of about 5 mm, while maintaining a similar level of vibration compared to the HS result. The same trend was also observed through an inspection of the corresponding flattening-D_{diff} curve in Fig. 10(b). Because the ovalization results are similar on both elbows, only those from one of the elbow are shown.

Concluding Remarks

In this paper, the seismic performance of a coupled structure-pipe-structure system typically found in an NG processing plant was

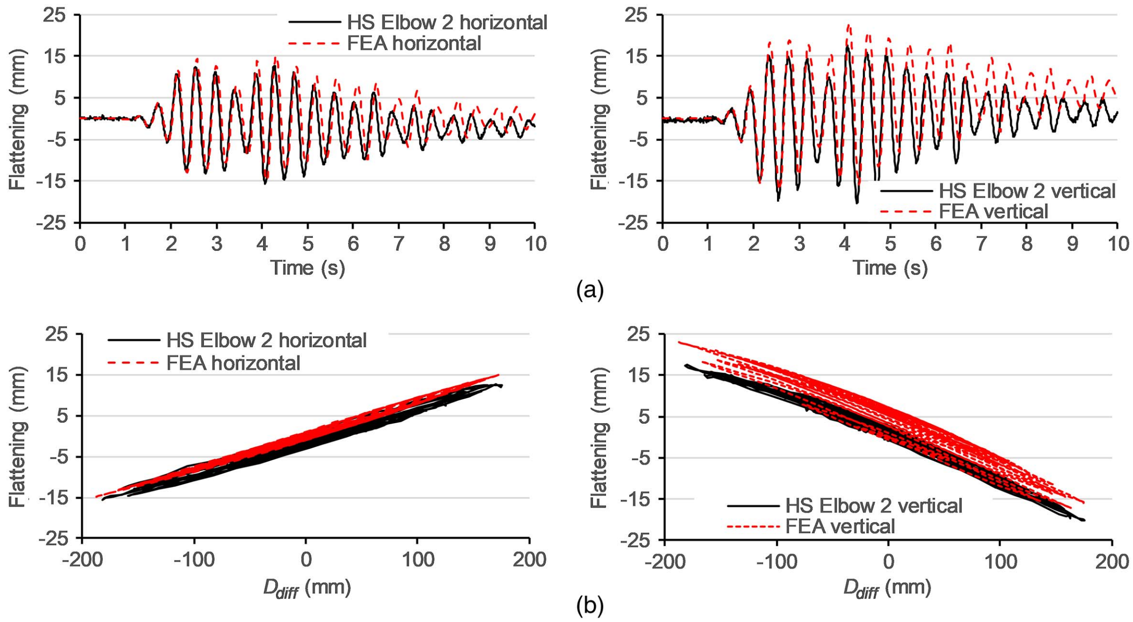

Fig. 10. Pipe cross-sectional ovalization response: (a) horizontal and vertical cross-sectional flattening versus time curves on Elbow 2 from the HS and the corresponding FE prediction; and (b) horizontal and vertical cross-sectional flattening versus D_{diff} curves on Elbow 2 from the HS and the corresponding FE prediction.

assessed by means of hybrid simulation (HS). A parametric study was firstly performed based on simplified FE models and the HS was conducted in which the holistic system was simulated as two coupled substructures so the linking NG pipe can be modeled physically in full-scale. Reliable boundary conditions of the linking NG pipe were established in our investigation by modeling explicitly the two supporting structures and analyzing the coupled structure-pipe-structure system as a holistic integer. Although the *x*-axis stiffness of the linking pipe element is much smaller than the swaying stiffness of the supporting structures, simulation results show a clear coupling effect introduced by its presence. Globally, differential displacement between the two supporting structures reduces up to 40% through the duration of the ground excitation for the reference analysis case due to the presence of the linking pipe element, indicating that the structure-pipe-structure interaction should not be overlooked for the proposed scenario and an HS is necessary for capturing the interaction experimentally. Locally, the connection of the linking pipe element to a total of two supporting structures with distinguishing dynamic properties contributes to the differential displacement between two pipe ends, hence the pronounced out-of-phase oscillation. As a result, the two pipe elbows can be bent severely into their nonlinear range.

The triggering factors of critical seismic demand for the linking NG pipe in the proposed structure-pipe-structure scenario are summarized as follows:

- The simultaneous mobilization of divergent structural oscillation at the low-frequency range between the two supporting structures: It leads to high responses both globally and locally, which can be attributed to the adverse combination of variable f_B/f_A, f_g, and H_p (i.e., natural frequency ratio of the supporting structures, predominant frequency of excitation, and the elevation of pipe-end attachment points). Peak differential displacement between two pipe ends, $D_{diff,max}$, and maximum local elbow hoop strain, $\epsilon_{h,max}$, are at their highest when the two supporting structures have different natural frequencies both in the low-frequency range and are both resonant to the input ground motion. Meanwhile, the elevation of pipe connecting points directly affects how much the linking pipe element can be exposed to the generated differential displacements between the two supporting structures, given the same input earthquake, the same structures, and the same pipe properties.
- A lower relative stiffness of the linking pipe element with respect to that of the structures: In general, a lower pipe-structure stiffness ratio leads to a lower structure-pipe-structure interaction, hence higher $D_{diff,max}$ and $\epsilon_{h,max}$ responses.
- Adverse geometry characteristic of linking pipe element: As the length of the straight pipe segments varies, the stiffness of the linking pipe element is barely affected. However, given the similar $D_{diff,max}$ responses, a linking pipe element with shorter straight pipe segments means that the two 90° elbows are more susceptible to bending, hence a higher seismic elbow strain demand.
- A higher pipe internal pressure P: The existence of pipe internal pressure naturally introduces a static load on the pipe, and hence, increases the elbow strain demand. Its potential benefit in mitigating excessive $D_{diff,max}$ response, thanks to the simultaneous pipe stiffness increase, is completely overshadowed by the increased pressure load itself.

Adjusting these variables to the unfavorable side can lead to significantly increased seismic demand to the pipe elbows. It is particularly true for the variables f_B/f_A and f_g, H_p, as well as P. Even when configuring only one of these variables from the reference scenario, which is a typical industrial site and is therefore deemed as a *probable* scenario, to a *worst-case* scenario, in which maximum responses were observed from the parametric study, can easily result in at least a 30% increase of the elbow strain demand.

Compared with the corresponding FE predictions, HS results show a peak differential displacement response between the two pipe ends of 189 mm and a maximum elbow hoop strain of 3.49% for the reference model. Pipe yielding, material plasticity, and strain ratcheting were observed on the elbows together with a clear asymmetric hysteretic behavior of the linking pipe element, which is mainly due to the nonlinear geometry of the linking pipe element and the ovalization of pipe cross section. On the other hand, pipe buckling or a loss of containment event did not occur under this level of elbow strain demand generated during the 7-s earthquake excitation of the HS.

Overall, the present study shows that the structure-pipe-structure interaction should not be overlooked, and we recommend a coupled analysis to be considered at least in the preliminary stage of future pipe-related studies in which similar structure-pipe-structure configurations are involved in a time history analysis, so that the imposed displacements at the boundary of the pipe segment are considered appropriately.

While numerical observations and the HS results were satisfactory, the study has some limitations, and thus, future works can be devoted to the following four directions. First, due to limited laboratory resources, the authors were only able to execute a single HS, which corresponds to the reference case of the parametric study. The limited stroke of the available hydraulic actuator also meant that an HS for any analysis case with a potentially higher dynamic structural response was not possible. Second, the presented numerical and experimental studies did not account for structural nonlinearity, soil-structure interaction, or a sophisticated modeling of pipe-end connection. Also, only a basic constitutive model was employed in the FE analyses to simulate the cyclic nonlinearity of the pipe steel material. Efforts can be put into those directions in the future, making use of refined FE models, to examine in greater detail the proposed structure-pipe-structure scenario. Third, investigations involving an extensive collection of earthquake ground motions can be made to derive fragility curves for the proposed scenario and gain deeper insight to the dynamic nature of the system in a probabilistic manner. Finally, given that the strain development on a steel pipe elbow is cumulative with regard to the total number of excitation cycles it undergoes, future work can be done to account for the effect of multiple earthquake events on the seismic elbow strain demand and its possible damage modes. This will address the potential seismic threat to steel NG pipe elbows in which they fail because of low cycle fatigue during their entire service life span after experiencing a number of strong ground motions, despite an immediate loss of pipe integrity in the form of buckling failure may not happen during a single earthquake event.

Data Availability Statement

Some or all data, models, or code that support the findings of this study are available from the corresponding author upon reasonable request. Items included are the ABAQUS finite-element models and scripts used in the parametric study, the numerical data from the parametric study, the OpenSees finite-element model used in the hybrid simulation, files and software associated with the UT-SIM framework used in the hybrid simulation, and the experimental data from the hybrid simulation.

Acknowledgments

This work was funded by the Horizon 2020 Programme of the European Commission through Grant MSCA-RISE-2015-691213-EXCHANGE-Risk (Experimental & Computational Hybrid Assessment of Natural Gas Pipelines Exposed to Seismic Risk, www.exchange-risk.eu). The first author also expresses his gratitude to the China Scholarship Council for financially supporting his doctoral studies (Grant No. 201808060061).

References

Bursi, O. S., R. di Filippo, V. La Salandra, M. Pedot, and M. S. Reza. 2018. "Probabilistic seismic analysis of an LNG subplant." *J. Loss Prev. Process Ind.* 53 (May): 45–60. https://doi.org/10.1016/j.jlp.2017.10.009.

CEN (European Committee for Standardization). 2006. *Eurocode 8: Design of structures for earthquake resistance—Part 4: Silos, tanks and pipelines eurocode*. EN 1998-4:2006. Brussels, Belgium: CEN.

Combescure, D., and P. Pegon. 1997. "α-Operator splitting time integration technique for pseudodynamic testing error propagation analysis." *Soil Dyn. Earthquake Eng.* 16 (7–8): 427–443. https://doi.org/10.1016/S0267-7261(97)00017-1.

DOE. 2017. *Understanding natural gas and LNG options*. Washington, DC: DOE.

Firoozabad, E. S., B.-G. Jeon, H.-S. Choi, and N.-S. Kim. 2015. "Seismic fragility analysis of seismically isolated nuclear power plants piping system." *Nucl. Eng. Des.* 284 (1): 264–279. https://doi.org/10.1016/j.nucengdes.2014.12.012.

Fouquiau, P.-V., F. Barbier, and C. Chatzigogos. 2018. "New dynamic decoupling criteria for secondary systems." In *Proc., 16th European Conf. on Earthquake Engineering*. Istanbul, Turkey: European Association for Earthquake Engineering.

GIE (Gas Infrastructure Europe). 2015. *Gas infrastructure Europe security risk assessment methodology.* Brussels, Belgium: GIE.

GIE (Gas Infrastructure Europe). 2019. *Gas infrastructure Europe LNG map 2019*. Brussels, Belgium: GIE.

Guarracino, F., A. Walker, and A. Giordano. 2009. "Effects of boundary conditions on testing of pipes and finite element modelling." *Int. J. Press. Vessels Pip.* 86 (2–3): 196–206. https://doi.org/10.1016/j.ijpvp.2008.09.009.

Gupta, A. K., and J. M. Tembulkar. 1984. "Dynamic decoupling of secondary systems." *Nucl. Eng. Des.* 81 (3): 359–373. https://doi.org/10.1016/0029-5493(84)90282-6.

Hasegawa, K., K. Miyazaki, and I. Nakamura. 2008. "Failure mode and failure strengths for wall thinning straight pipes and elbows subjected to seismic loading." *J. Pressure Vessel Technol.* 130 (1): 1–8. https://doi.org/10.1115/1.2826425.

Hassan, T., M. Rahman, and S. Bari. 2015. "Low-cycle fatigue and ratcheting responses of elbow piping components." *J. Pressure Vessel Technol.* 137 (3): 1–12. https://doi.org/10.1115/1.4029068.

Huang, X., and O.-S. Kwon. 2018. "A generalized numerical/experimental distributed simulation framework." *J. Earthquake Eng.* 24 (4): 682–703. https://doi.org/10.1080/13632469.2018.1423585.

Jeon, B.-G., S.-W. Kim, H.-S. Choi, D.-U. Park, and N.-S. Kim. 2017. "A failure estimation method of steel pipe elbows under in-plane cyclic loading." *Nucl. Eng. Technol.* 49 (1): 245–253. https://doi.org/10.1016/j.net.2016.07.006.

Karamanos, S. A. 2016. "Mechanical behavior of steel pipe bends: An overview." *J. Pressure Vessel Technol.* 138 (4): 1–15. https://doi.org/10.1115/1.4031940.

Karvelas, C., N. Stathas, E. Strepelias, X. Palios, G. Chatzopoulou, S. Bousias, and S. Karamanos. 2019. "Strong cyclic loading of an industrial piping system." In *Proc., 2nd Int. Conf. on Natural Hazards & Infrastructure*. Athens, Greece: National Technical Univ. of Athens.

Lanzano, G., F. Santucci de Magistris, G. Fabbrocino, and E. Salzano. 2015. "Seismic damage to pipelines in the framework of Na-Tech risk assessment." *J. Loss Prev. Process Ind.* 33 (Jan): 159–172. https://doi.org/10.1016/j.jlp.2014.12.006.

Mazzoni, S., F. McKenna, M. H. Scott, and G. L. Fenves. 2006. *Open system for earthquake engineering simulation (OpenSees)—OpenSees command language manual*. Berkeley, CA: Univ. of California, Berkeley.

Molina, F. J., G. Magonette, P. Pegon, and B. Zapico. 2011. "Monitoring damping in pseudo-dynamic tests." *J. Earthquake Eng.* 15 (6): 877–900. https://doi.org/10.1080/13632469.2010.544373.

Mortazavi, P., X. Huang, O.-S. Kwon, and C. Christopoulos. 2017. *Example manual for University of Toronto simulation (UT-SIM) framework. An open-source framework for integrated multi-platform simulations for structural resilience*. 2nd ed. Toronto, Canada: Univ. of Toronto.

Nakamura, I., and N. Kasahara. 2016. "Trial model tests with simulation material to obtain failure modes of pipes under excessive seismic loads." In *Proc., ASME 2016 Pressure Vessels and Piping Conf.*, 1–11. New York: ASME. https://doi.org/10.1115/PVP2016-63422.

Nakamura, I., and N. Kasahara. 2017. "Excitation tests on elbow pipe specimens to investigate failure behavior under excessive seismic loads." *J. Pressure Vessel Technol.* 139 (6): 1–11. https://doi.org/10.1115/1.4037952.

Nakashima, M., O. Lavan, M. Kurata, and Y. Luo. 2014. "Earthquake engineering research needs in light of lessons learned from the 2011 Tohoku earthquake." *Earthquake Eng. Eng. Vibr.* 13 (1): 141–149. https://doi.org/10.1007/s11803-014-0244-y.

Park, J., Z. Zhang, O. Kwon, S. Bousias, and A. Sextos. Forthcoming. "Hybrid testing for assessing the coupled seismic response of a natural gas pipeline linking two structures within a pressurising station." In *Proc., 17th World Conf. on Earthquake Engineering*. Hoboken, NJ: Wiley. http://www.exchange-risk.eu/uploads/4/3/9/4/439426/pipe_hybrid_testing_-_conference_paper_finalized1.pdf.

Psyrras, N., O. Kwon, S. Gerasimidis, and A. Sextos. 2019. "Can a buried gas pipeline experience local buckling during earthquake ground shaking?" *Soil Dyn. Earthquake Eng.* 116 (Jan): 511–529. https://doi.org/10.1016/j.soildyn.2018.10.027.

Psyrras, N., A. Sextos, A. Crewe, M. Dietz, and G. Mylonakis. 2020. "Physical modeling of the seismic response of gas pipelines in laterally inhomogeneous soil." *J. Geotech. Geoenviron. Eng.* 146 (5): 04020031. https://doi.org/10.1061/(ASCE)GT.1943-5606.0002242.

Reza, M. S., O. S. Bursi, G. Abbiati, and A. Bonelli. 2013. "Pseudo-dynamic heterogeneous testing with dynamic substructuring of a piping system under earthquake loading." In Vol. 8 of *Proc., ASME 2013 Pressure Vessels and Piping Conf.* New York: ASME.

Ricker, N. 1943. "Further developments in the wavelet theory of seismogram structure." *Bull. Seismol. Soc. Am.* 33 (3): 197–228.

Sakai, M., S. Matsuura, and F. Inada. 2013. "Hybrid seismic response evaluation method for wall thinning piping system." In Vol. 1 of *Proc., 21st Int. Conf. on Nuclear Engineering*. New York: ASME.

Sextos, A., et al. 2018. "Exchange-risk: Experimental & computational hybrid assessment of natural gas pipelines exposed to seismic risk." In *Proc., 16th European Conf. on Earthquake Engineering*, 1–12. Istanbul, Turkey: European Association for Earthquake Engineering.

Sextos, A., G. Manolis, N. Ioannidis, and A. Athanasiou. 2017. "Seismically induced uplift effects on nuclear power plants. Part 2: Demand on internal equipment." *Nucl. Eng. Des.* 318 (Jul): 288–296. https://doi.org/10.1016/j.nucengdes.2016.12.036.

Shalaby, M. A., and M. Y. A. Younan. 1998. "Limit loads for pipe elbows with internal pressure under in-plane closing bending moments." *J. Pressure Vessel Technol.* 120 (1): 35–42. https://doi.org/10.1115/1.2841882.

Taghavi, S., and E. Miranda. 2008. "Effect of interaction between primary and secondary systems on floor response spectra." In *Proc., 14th World Conference on Earthquake Engineering*. Tokyo: International Association for Earthquake Engineering.

Varelis, G. E., S. A. Karamanos, and A. M. Gresnigt. 2012. "Pipe elbows under strong cyclic loading." In Vol. 8 of *Proc., ASME 2012 Pressure Vessels and Piping Conf.*, 45–54. New York: ASME.

Varelis, G. E., P. Pappa, and S. A. Karamanos. 2011. "Finite element analysis of industrial steel elbows under strong cyclic loading." In Vol. 8 of *Proc., ASME 2011 Pressure Vessels and Piping Conf.*, 109–119. New York: ASME.

Vathi, M., S. A. Karamanos, I. A. Kapogiannis, and K. V. Spiliopoulos. 2017. "Performance criteria for liquid storage tanks and piping systems subjected to seismic loading." *J. Pressure Vessel Technol.* 139 (5): 1–12. https://doi.org/10.1115/1.4036916.

Vazouras, P., S. A. Karamanos, and P. Dakoulas. 2010. "Finite element analysis of buried steel pipelines under strike-slip fault displacements." *Soil Dyn. Earthquake Eng.* 30 (11): 1361–1376. https://doi.org/10.1016/j.soildyn.2010.06.011.

Watakabe, T., I. Nakamura, A. Otani, M. Morishita, T. Shibutani, and M. Shiratori. 2017. "Seismic qualification of piping systems by detailed inelastic response analysis: Part 4—Second round benchmark analyses with stainless steel piping component test." In Vol. 8 of *Proc., ASME 2017 Pressure Vessels and Piping Conf.* New York: ASME.

Wenzel, M., F. Basone, and O. S. Bursi. 2018. "Novel metamaterial-based foundation concept applied to a coupled tank-pipeline system." In Vol. 5 of *Proc., ASME 2018 Pressure Vessels and Piping Conf.*, 1–12. New York: ASME.

Yoshizaki, K., M. Hamada, and T. O'Rourke. 2000. "Large deformation behavior of low-angle pipeline elbows subjected to in-plane bending." In Vol. 1508 of *Proc., 12th World Conf. on Earthquake Engineering*. Tokyo: Association for Earthquake Engineering.

Zhan, H., and O.-S. Kwon. 2015. "Actuator controller interface program for pseudo- dynamic hybrid simulation." In *Proc., 2015 World Congress on Advances in Structural Engineering and Mechanics*, 1–13. Daejeon, Korea: International Association of Structural Engineering and Mechanics.